# Reduced-scale lab experiments : a valuable tool for exploring current challenges of seismic surveying, modeling and imaging in complex marine environments at a low cost and in an agile way ?

Nathalie Favretto-Cristini, Bence Solymosi, Vadim Monteiller, Paul Cristini, Bjorn Ursin

# REDUCED-SCALE LAB EXPERIMENTS : A VALUABLE TOOL FOR EXPLORING CURRENT CHALLENGES OF SEISMIC SURVEYING, MODELING AND IMAGING IN COMPLEX MARINE ENVIRONMENTS AT A LOW COST AND IN AN AGILE WAY ?

**N. Favretto-Cristini**[1] **B. Solymosi**[1] **V. Monteiller**[1]
**P. Cristini**[1] **B. Ursin**[2]
[1] Aix-Marseille Univ, CNRS, Centrale Marseille, LMA, France
[2] NTNU, Department of Electronic Systems, Trondheim, Norway
favretto@lma.cnrs-mrs.fr

## ABSTRACT

Recently, lab experiments have been reintroduced in the ideas-to-applications pipeline for geophysical issues. Benefiting from recent technological advances, lab experiments may play a major role in the coming years, in support of field experiments and numerical modeling, to explore some of the current challenges of seismic imaging in terms of, for instance, acquisition design or benchmarking of new imaging techniques at a low cost and in an agile way. But having confidence in the quality and the accuracy of the experimental data obtained in a complex configuration that mimics at a reduced scale a real geological environment is an essential prerequisite. This requires a robust framework regardless of the configuration studied. The goal of this work is to provide a global reflection on this framework in the context of offshore seismics. To illustrate this framework, we rely on different reduced-scale models, and more specifically on a model that represents a 3D complex-shaped salt body buried in sedimentary layers with curved surfaces. Zero-offset and offset reflection data are collected on this model in a water tank, using a conventional pulse-echo technique. We follow a cross-validation approach that allows, through the comparison between the experimental data and the numerical simulation of wave propagation, to point out both the improvements of the experimental setup that must still be made to increase the accuracy of the experiments, and the limitations of the numerical tools that must be tackled. This framework can however be used with confidence to investigate cutting-edge seismic issues in complex environments.

## 1. INTRODUCTION

Numerical simulation of wave propagation is a core tool of seismic imaging and inversion in subsurface exploration. It is also used to improve seismic surveys and to explore seismic acquisition designs and imaging techniques in challenging geological environments. However, it is difficult to study and improve surveying and imaging using fully numerical settings only, because numerical datasets usually suffer from simplified physics, since they do not contain, for instance, source-related noise, or sometimes contain "unphysical" attenuation parameters however considered in numerical tools. On the other hand, relying on real seismic datasets only is tricky as well, because reliable datasets are always costly, sometimes incomplete or difficult to access, and rarely perfectly controlled. In this context, without substituting for real seismic data, reduced-scale data obtained in controlled lab conditions are a very interesting alternative which we can play with.

Lab experiments are now considered again as a good support to real data and to purely numerical data, in order to significantly contribute to test new ideas [1], to investigate the physics underlying wave propagation that is not sufficiently understood [2], as well as to test numerical algorithms used for data processing and imaging [3]. Recently, small-scale modeling approaches have been developed as tools to test numerical modeling and seismic-imaging methods in the context of onshore and offshore seismics [4–6]. In particular, Tantsereva et al. [5] have evaluated the ability of a 3D discretized Kirchhoff integral method (DKIM) to accurately simulate complex diffractions using a zero-offset lab data set, measured for a reduced-scale model with strong topography and immersed in a water tank. Comparisons of numerical and lab data sets have shown that the DKIM could correctly reproduce the wavefield, except in the vicinity of secondary shadow boundaries created by the interaction of the edges of the topographic structures. More importantly, a quantitative analysis of the effect of multiple scattering and the surface curvature on the wavefield has been then performed to define the cases where these effects may be neglected in numerical modeling, in order to decrease the computational cost while maintaining a high degree of result accuracy [7]. These works clearly show the importance of lab experiments as part of the benchmarking options for numerical algorithms. Indeed, without substituting to real data, reduced-scale experiments are highly valuable because they can be repeatable, more controllable than real seismic surveys, and versatile in terms of acquisition setups. Because the sources and the level of noise, as well as the uncertainties due to source and receiver position inaccuracies or associated with the media properties, can be better assessed than in the case of field data sets, lab ex-

periments also provide higher fidelity data than real seismic surveys. We believe that reduced-scale models with realistic complexity from a geological viewpoint, associated with a very high quality and accurate lab experimental framework, could in the near future be one of the cornerstones for exploring some of the current challenges of seismic imaging in terms of acquisition design, or for benchmarking new imaging techniques at a low cost and in an agile way. But having confidence in the quality and in the accuracy of the experimental data obtained in a very complex environment is an essential prerequisite. As a consequence, this requires a robust framework regardless of the configuration studied.

Here, we present this framework based on the cross-validation approach between numerical tools and a lab setup: comparison between numerical and experimental results emphasizes the improvements of the experimental setup that must be made to increase the accuracy (and decrease the uncertainties) of the experiments, and at the same time, points out the limitations of the numerical tool that must be tackled. To illustrate this framework, we rely on a much more complex case study that is also much more realistic from a geological viewpoint than the configuration considered in our previous works [5, 6] or configurations considered in other works (e.g. [2, 8]), namely a complex-shaped salt body buried in sedimentary layers with curved surfaces. This choice is motivated by the fact that salt structures usually play a crucial role in hydrocarbon migration and entrapment, and despite advances in migration algorithms and inversion methods, accurate (sub-)salt imaging is still an ongoing challenge for seismic exploration [9]. We have thus built the WAVES reduced-scale model (scale ratio $1:20\,000$) that closely represents both the geometry and the media properties of a realistic 3D geologic setup, using specific materials such as specific crystal and resins. Zero-offset and offset reflection datasets have been then collected for this reduced-scale model in a water tank, using a conventional pulse-echo technique and a broadband/broadbeam piezoelectric transducer and a hydrophone. In order to identify the points that need particular attention to allow lab experiments to be very efficient tools in support of real data and numerical simulations for seismic exploration issues, we have compared these experimental datasets to corresponding numerical data obtained using a full-wave method, namely a spectral-element method (SEM) [10]. To be effective, this cross-validation requires that the same input data (e.g. the geometry and the physical properties of the model, the characteristics of the sources and the receiver, the acquisition design...) have to be considered carefully in both the experiments and the numerical tool.

The paper is then organized as follows. Section 2 is devoted to the reduced-scale modeling, including the description of the WAVES model and the lab experiments. In Section 3 the principles of the SEM used for obtaining numerical data similar to lab data are briefly recalled. The numerical implementation of the input data similar to lab conditions is also discussed here. Section 4 presents the comparison between the lab data and the corresponding numerical results, and widely discusses the possible origins of the observed misfits. Despite the (small) misfits, the whole framework is validated and confirms the high potential of lab experiments for cutting-edge seismic imaging and acquisition issues in complex environments.

## 2. REDUCED-SCALE SEISMIC MODELING

### 2.1 The WAVES model

The real-life dimensions are scaled down to the lab scale by a factor of $1:20\,000$. Therefore 1 mm at the lab scale corresponds to $20\,m$ at seismic scale. The WAVES reduced-scale model has a size of $400$x$270$x$95\,mm$, which corresponds to $8$x$5.4$x$1.9\,km$ at seismic scale. The model mimics a salt-body embedded in sedimentary layers (Figure 1). Salt is represented by crystal, and the sediments are represented by resins (Table 1). The resins are all based on the same base material, but some of them are enriched with a mixture of aluminum and silicon dioxide powder to increase their density and the wave velocities. The aluminum layer on the bottom represents a typical crystalline basement, such as granite. The P- and S-wave velocity and attenuation values (expressed as $Q$-factors), obtained with transmission measurements through two material samples of different thickness, are close to constant within the frequency range of interest ($250 - 650\,kHz$). Each material is therefore considered to be homogeneous and isotropic for the frequency range of interest (Table 1). We consider glass and aluminum to be elastic, i.e. $Q_P$ and $Q_S$ are infinite.

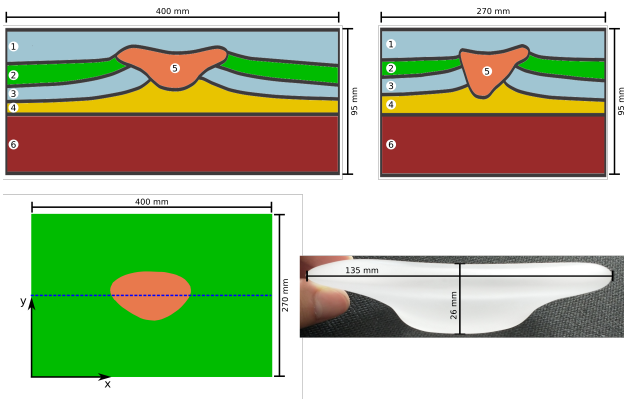


**Figure 1**. The WAVES model. Top : perpendicular vertical cross-sections along the center lines of the model. The numbers denote the materials whose properties are reported in Table 1. Bottom : top view of the model without the topmost layer, the blue dashed line denotes the study line discussed in the paper (left), the glass dome placed inside the model (right).

### 2.2 Experimental setup

Because the objective was to perform reduced-scale offshore seismic acquisitions, the WAVES model was immersed in a water tank before the measurements (Figure

| Layer (Number in Fig 1) | $\varrho$ $(\mathrm{kg/m^3})$ | $V_P$ $(\mathrm{m/s})$ | $V_S$ $(\mathrm{m/s})$ | $Q_P$ | $Q_S$ |
|---|---|---|---|---|---|
| Resin A (#1,3) | $1\,172 \pm 2$ | $2\,720 \pm 13$ | $1\,210 \pm 144$ | $25 \pm 1$ | $11 \pm 4$ |
| Resin B (#2) | $1\,680 \pm 10$ | $3\,090 \pm 16$ | $1\,577 \pm 25$ | $26 \pm 1$ | $18 \pm 3$ |
| Resin C (#4) | $1\,800 \pm 10$ | $3\,470 \pm 21$ | $1\,840 \pm 101$ | $53 \pm 1$ | $33 \pm 9$ |
| Crystal (#5) | $3\,623 \pm 10$ | $4\,480 \pm 43$ | $2\,845 \pm 464$ | $\infty$ | $\infty$ |
| Aluminum (#6) | $2\,710 \pm 4$ | $6\,441 \pm 87$ | $3\,573 \pm 544$ | $\infty$ | $\infty$ |

**Table 1**. Measured properties of the materials used in the WAVES model, together with the associated uncertainties for the frequency range (250–650 kHz).

2). The tank is equipped with a computer-controlled acquisition system that allows for the accurate positioning of the ultrasonic transducers. Compared to the experimental setup described in [6], the precision of the measurements has been significantly improved thanks to optic rulers that provide a precise a posteriori control of the transducer movements, as well as a digital protractor that measures the tilt angle of the source transducer. The precision of the transducer movement and that of the source tilt angle have thus been improved by a factor of 100 and 10, respectively. The uncertainty of the transducer movements has thus been reduced to $\pm\,5\,\mu m$ (i.e. $\pm\,0.1\,m$ at seismic scale), while the tilt angle of the source transducer can now be measured with a precision of $\pm\,0.1°$. However, determining with high accuracy the initial position of both the transducer and the hydrophone before the data acquisition is still problematic. So far, this accuracy cannot be below $0.5\,mm$. This is definitely a point to further investigate and improve in our future works.

As in [6], we used a conventional pulse-echo technique to collect reflection data in both zero-offset and offset configurations. Zero-offset data was acquired using a custom-made Imasonic transducer as both the source and the receiver. This transducer has a dominant frequency of $500\ kHz$ (i.e. $25\ Hz$ at seismic scale) and a broad-beam radiation pattern. Because the width of the main lobe is $35°$ at $-3\,dB$, this transducer has a large illumination area, leading to a complex 3D wavefield [5]. In the offset configuration an omnidirectional Teledyne Reson hydrophone that has a constant sensitivity for the frequency range of interest was used as the receiver. For more details on the lab measurements, we refer the reader to [6].

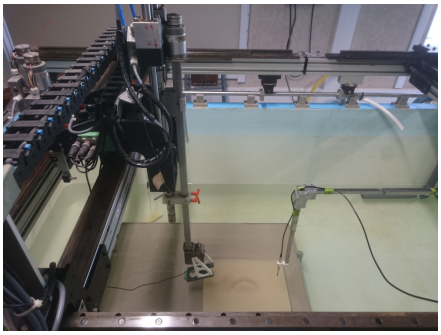

**Figure 2**. Offset data acquisition setup showing the source and the receiver, respectively on the left and right side of the WAVES model in the water tank.

### 2.3 Laboratory data sets

For the sake of brevity, we focus on a study line, located above the center line in the x-direction (dashed line in Figure 1 bottom left). This acquisition line covers both rather simpler parts close to the sides where the geometry consists of close-to-horizontal layers, and complex parts in the center above the dome.

Figure 3 shows the lab zero-offset data set for the study line together with the interpretation of the main recorded events. The transducer was positioned $100 \pm 0.1\,mm$ above the top surface of the model (i.e. $2\,000 \pm 2\,m$ at seismic scale) and recorded events every $0.5\,mm$ in the x-direction. Event a) represents the reflections from the top surface of the model, i.e. from the top of the upper resin A layer. Event b) represents mainly the reflections from the top of the glass dome, in particular for positions $120-270\,mm$. For positions less than $120\,mm$ and greater than $270\,mm$ diffractions from the edges of the dome can also be observed. Events c), d), e), and f) are associated with the top surface of resin B, lower resin A, resin C, and aluminum, respectively. These events can be easily interpreted on the sides due to the relatively simple geometry. On the contrary, the closer we are to the center of the model, the harder it is to distinguish the same reflections due to the complex geometry. Thanks to the broad-beam radiation pattern of the source transducer and the curved top surface of the dome, we can see a constructive interference of reflections in the center, leading to focusing of the energy, between $165 - 200\,\mu s$ and between positions $170 - 240\,mm$. Event g) shows reflections from the bottom of the aluminum. The fact that reflections are recorded from the bottom of the aluminum shows that the imaging of the entire depth of the model is possible, even though the resin layers are very attenuating. Although events f) and g) represent reflections from two perfectly horizontal interfaces, they exhibit some undulations in Figure 3, which is indeed a velocity pull-up effect due to the time-domain visualization. This is the result of the varying velocity of the complex overburden of the aluminum, which then leads to different arrival times of the reflected zero-offset waves at different horizontal positions.

Figure 4 shows the lab offset data set for the study line, i.e. a common shot gather, together with the interpretation of the main events. The source was positioned at $y = 390.2 \pm 0.5\,mm$ and the tilt angle of the source transducer was $30° \pm 0.1°$. Both the source and the receiver transducers were positioned $100 \pm 0.1\,mm$ above

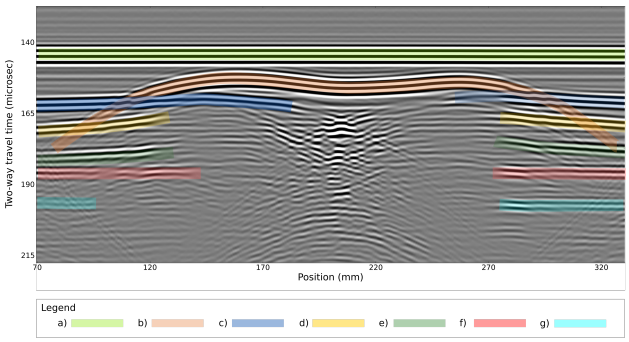


**Figure 3**. Cross-section of the lab zero-offset data set along the study line and interpretation. Annotated events: reflections from the (a) top of the upper resin A layer, (b) top of the glass dome, (c) top of the resin B layer, (d) top of the lower resin A layer, (e) top of the resin C layer, (f) top of the aluminum layer, and (g) bottom of the aluminum layer. The data was filtered between 250-650 kHz.

the top surface of the model (i.e. $2\,000 \pm 2\,m$ at seismic scale). The hydrophone was moved every $0.5\,mm$ in the x-direction to record events. The interpretation of the measured data set for the WAVES model without post-processing is challenging due to the complex multi-layered geometry. Nevertheless, event a) can be unambiguously attributed to the direct arrival from the source, and event b) to the reflections from the top surface of the model, i.e. from the top of the upper resin A layer. To go further in the interpretation, the laboratory data must be post-processed, most typically with migration algorithms. We show an example of this post-processing subsequently.

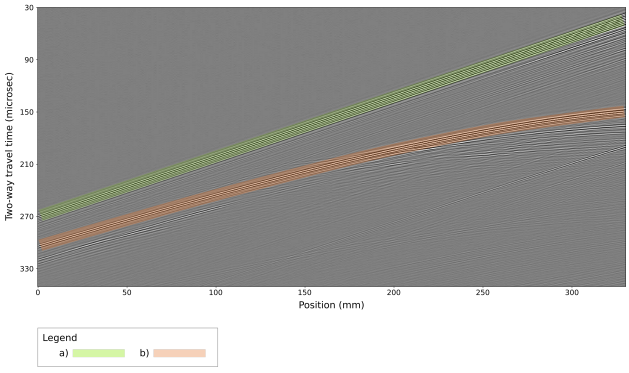


**Figure 4**. Cross-section of the lab offset data set along the study line (i.e. common shot gather) and interpretation. Annotated events: (a) direct arrival, (b) reflection from the top of the upper resin A layer. The data was filtered between 250-650 kHz.

## 3. NUMERICAL MODELING

### 3.1 Brief description of the spectral-element method

We resorted to the spectral-element method (SEM) for the numerical simulations. Specifically, we used the Specfem software package [10] with the explicit second-order Newmark time scheme. The numerical modeling is conducted in the same way as reported in [6], including the implementation of the viscoelasticity and the implementation of the real wide-beam source signal and radiation pattern. The only difference lies in the implementation of the model geometry. Because the WAVES model has a complex 3D multi-layered geometry, obtaining a non-structured hexahedral mesh is extremely difficult. The main difficulty is not only to correctly mesh any domain of the model with hexahedral elements only, but also to have a conformal mesh on the boundaries between any two domains. Indeed, in a conform mesh all nodes which are on the boundary of two domains are shared by elements on both sides, and all elements on the boundaries must be connected to elements in the other domain by nodes. Although several open-source and commercial meshing software were tested, currently they are all unable to tackle this task for the WAVES model. Because a conform mesh is necessary for the numerical simulations, we had to choose a different approach to numerically implement the model geometry, namely, a structured grid. Considering the minimum velocity of the model – namely, $1\,210\ \mathrm{m/s}$ for the S-waves in resin A – and the maximum target frequency ($650\,kHz$), we used a grid with an equidistant grid spacing of $1.6\,mm$ in each spatial direction. Because five Gauss-Lobatto-Legendre (GLL) points per element are used during the simulations, the grid spacing provides at least 7.1 and 5.8 GLL points per the shortest wavelength for P- and S-waves, respectively. This spatial discretization yields approximately 5.6 million elements, considering the water column above the model as well.

### 3.2 Numerical calibration of the material properties for a multi-layered model

Because the ultrasonic characterization of the material samples yields a range of possible values for the measured properties due to the measurement uncertainties, an initial calibration is necessary to find the relevant values to be used for the simulations. The calibration consists of a zero-offset lab measurement, followed by an iterative fitting of the corresponding synthetic trace. This iterative fitting consists in adjusting the material parameters of each layer such that the simulation yields the closest possible fit with the reference laboratory trace. The WAVES model is challenging due to its multi-layered geometry. So, at first, the properties of the topmost layer are calibrated, then, considering these calibrated values, the properties of the second layer are calibrated, and so on. We chose a reference point $100 \pm 0.1\,mm$ above the top surface of the model as close to the sides of the model as possible where the geometry is close to a 2D layer-cake geometry, but avoiding diffractions effects from the model edges (Figure 5). The calibration thus consists of two phases: first, the properties of each layer except those of the glass dome are calibrated successively using the reference point, then, a second trace is used in the center of the model to fit the properties of the glass too.

Figure 6a shows the comparison of the reference lab trace with the simulated trace, using the measured mate-

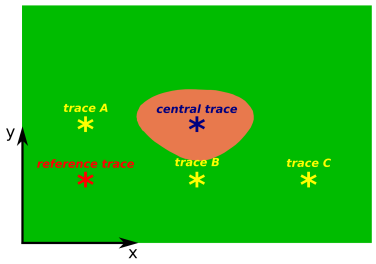


**Figure 5**. Location of the reference trace (red asterisk) and of the second trace used to calibrate the properties of the glass (blue asterisk). The yellow asterisks denote the position of the zero-offset examples showcased hereafter.

rial properties reported in Table 1. Although the arrival time, amplitude and phase of the simulation are correct for the first event (reflection from the top of the upper resin A layer), the later arrivals have extremely low amplitudes compared to the lab measurement. By successively adjusting the material parameters of the different layers, we can finally obtain an excellent fit between the lab and synthetic traces, as shown in Figure 6b, from both a qualitative and a quantitative (through correlation coefficients) viewpoints. Table 2 reports the adjusted material properties and the change in terms of percentage compared to the measured material properties listed in Table 1. At this point, we have to note that the differences between the adjusted and the measured values of the $Q$-factors can be significant, whereas the differences in the velocity values remain small. Moreover, even though the same resin A is used twice in the model, we obtained different material properties for the upper and lower layers, especially for the attenuation parameters. Finally, using the calibrated material properties of Table 2, we did an additional control measurement and simulation in the same horizontal position, but one centimeter closer to the surface of the model (i.e. at $90 \pm 0.1\,mm$ above the top surface of the model). Changing only the height of the transducer results in a slightly different fit between lab and synthetic traces (Figure 7). It can be explained by the fact that the width of the illuminated zone of the model changes with the transducer height. We can clearly see here the importance of the illuminated zone on the measurements, and on the calibration as well, in particular for a multi-layered medium. Thus the adjusted material parameters should be considered here as rather apparent or effective parameters than intrinsic parameters of the materials.

After calibrating the material properties for the resins and the aluminum, a second trace was used in the center of the model to adjust the properties of the glass (blue asterisk in Figure 5). Figure 8a shows the comparison of the lab trace with the synthetic results, using the adjusted material properties listed in Table 2. We can see that the two traces fit each other very well for the reflection from the top of the upper resin A layer. Figure 8b shows the same comparison, but this time the material properties of the glass dome are also calibrated (Table 2). We can clearly see a good

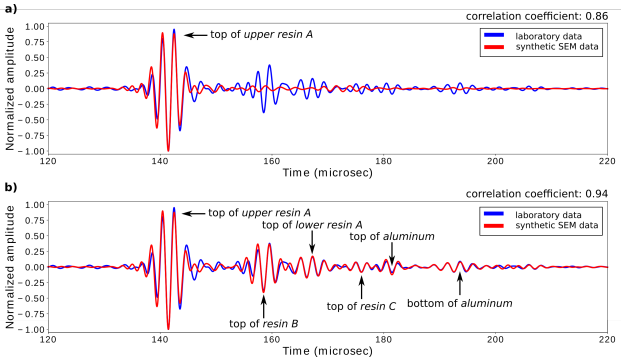


**Figure 6**. Comparison of the reference lab trace (blue) and the corresponding synthetic trace (red) obtained using: a) the measured material properties reported in Tab. 1, b) the adjusted material properties reported in Tab. 2.

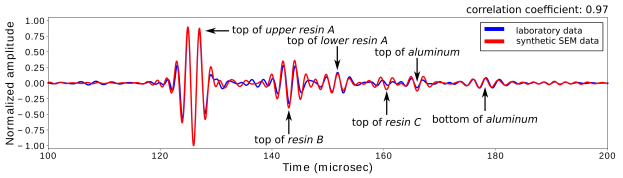


**Figure 7**. Comparison of the lab trace (blue) recorded at the same horizontal position as the reference trace (Fig. 6), but one centimeter closer to the model, and the corresponding synthetic trace (red) obtained using the adjusted material properties reported in Tab. 2.

fit between the lab and synthetic traces for the reflection from the bottom of the glass dome too, as well as for other events with later arrival times. The reflection from the top of the glass dome shows a good, but not a perfect fit, as the amplitude is overestimated compared to the lab measurement. To decrease this misfit, the properties of upper resin A should have been readjusted. This does not mean that the layer is heterogeneous, but rather that the effect of the illuminated zone also depends on the model geometry (especially in this case when the top surface of the dome is curved).

## 4. COMPARISON BETWEEN EXPERIMENTAL AND NUMERICAL DATA

### 4.1 Comparison of zero-offset data

In addition to the reference and the central traces, we have considered more specifically three traces of the lab zero-offset data set, denoted with the yellow asterisks in Fig. 5. These traces are located at different parts of the model to investigate the fit between the measurements and the simulations, using the calibrated material properties (Table 2) at different positions. For the sake of brevity, we present here the results obtained for Trace B only. This trace is located about $130\,mm$ (i.e. $2.6\,km$ at seismic scale) far from the reference trace in the x-direction. Figure 9 shows a good fit between the measurements and the simulations for the reflection from the top of the upper resin A layer,

| Layer | $\varrho$ $(\mathrm{kg/m^3})$ | $V_P$ $(\mathrm{m/s})$ | $V_S$ $(\mathrm{m/s})$ | $Q_P$ | $Q_S$ |
|---|---|---|---|---|---|
| Resin A (#1) | 1 172 (0 %) | 2 549 (−6 %) | 1 210 (0 %) | 124 (376 %) | 88 (389 %) |
| Resin B (#2) | 1 680 (0 %) | 3 213 (4 %) | 1 577 (0 %) | 27 (5 %) | 23 (28 %) |
| Resin A (#3) | 1 172 (0 %) | 2 560 (−6 %) | 1 210 (0 %) | 42 (60 %) | 30 (67 %) |
| Resin C (#4) | 1 800 (0 %) | 3 050 (−12 %) | 1 840 (0 %) | 30 (−43 %) | 26 (−21 %) |
| Crystal (#5) | 3 623 (0 %) | 4 325 (−4 %) | 2 845 (0 %) | $\infty$ (0 %) | $\infty$ (0 %) |
| Aluminum (#6) | 2 710 (0 %) | 6 491 (< 1 %) | 3 573 (0 %) | $\infty$ (0 %) | $\infty$ (0 %) |

**Table 2**. The calibrated material properties for the different layers. The percentages show the differences compared to the measured values listed in Tab. 1.

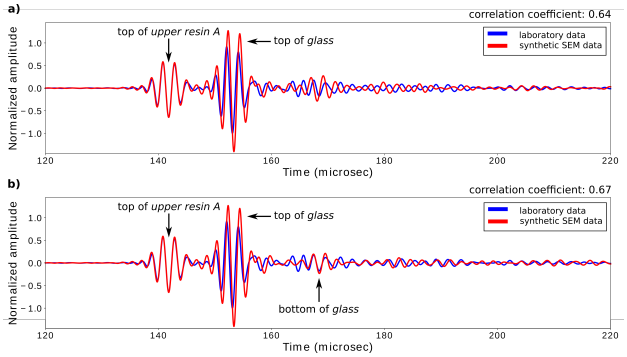


**Figure 8**. Comparison of the lab trace (blue) recorded in the center of the model and the corresponding synthetic trace (red) obtained using the adjusted material properties listed in Tab. 2 : a) except , b) including those of the glass dome.

except for the tail of the event which exhibits some minor amplitude misfits. Although some amplitude misfits can be observed, the reflections from the top of resin B and lower resin A layers are well restored by the simulations. On the contrary, the later arrivals of the trace (corresponding to reflections from the top of the resin C layer and to reflections from the top and bottom of the aluminum layer) show an almost perfect fit in both the arrival times and the amplitudes. Despite the occasional amplitude misfits, this trace has a high correlation coefficient (0.87).

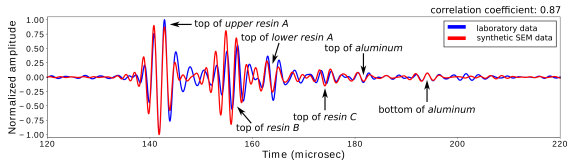


**Figure 9**. Comparison of a zero-offset lab trace (trace B on Fig. 5) with the corresponding synthetic SEM result.

### 4.2 Comparison of offset data

We have also considered two sets of offset traces corresponding to two different source positions. All the sources and receivers were positioned in the center line of the model in the y-direction $y = 135 \pm 0.5\,mm$. The two source positions are denoted with red and blue asterisks in Figure 10, respectively. The positions of the receivers are denoted with triangles of the corresponding color. The tilt angle of the source transducer for all the traces was $31.3° \pm 0.1°$. For the sake of brevity, we show here only a couple of traces, namely Traces D and E. For these traces, the source was positioned at $x = 300 \pm 0.5\,mm$ (Figure 10). Trace D corresponds to an offset of $280 \pm 0.5\,mm$ (i.e. $5.6 \pm 0.01\,km$ at seismic scale), while Trace E was recorded at an offset of $80 \pm 0.5\,mm$ (i.e. $1.6 \pm 0.01\,km$ at seismic scale). Figure 11 shows the comparison of the lab measurements with the synthetic results. For Trace D, the reflection from the top of the upper resin A layer shows a good fit between the two traces, in terms of both the arrival time and the amplitude. Although the arrival time of the reflection from the top of the glass dome is correct for the synthetic trace, the simulated amplitude is somewhat lower compared to the measurement. The later arrivals which propagated through the glass dome cannot be easily interpreted one-by-one, because they belong to complex ray paths. Although the arrival time and phase of these events are correct, they show a varying amplitude misfit. The correlation coefficient of 0.84 however suggests a generally good fit between the measurement and the simulation. For Trace E, the comparison of the measured and simulated traces shows a good fit for the reflection from the top of the upper resin A layer, similar to trace D. Following that, there are two arrivals corresponding to reflections from the top of the glass dome. This is due to the broad-beam radiation pattern of the source in combination with the curved top surface of the dome. These arrivals show some arrival time and amplitude misfits. The later arrivals, corresponding to waves propagating through the glass dome, show a similar pattern as for trace D. Namely, the arrival time of these events are mostly correct with some amplitude misfits. The correlation coefficient is 0.81, partly due to the erroneously low simulated amplitude of the later arrivals (e.g. at 180 $\mu s$).

### 4.3 Discussion

As shown above, we can accurately reconstruct the lab measurements for the WAVES model using the SEM with a regular grid. In general, a very good fit can be obtained between the lab zero-offset measurements and the numerical simulations. Although the observed misfits are somewhat higher in the offset configuration, the values of the correlation coefficients still suggest a good reconstruction of the lab offset traces as well. At this point, it is interesting to focus on the possible origins of the observed misfits, and to evaluate as much as possible the associated uncertain-

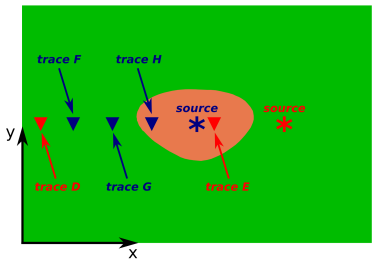


**Figure 10**. Location of the sources (asterisk) and receivers (triangles) associated to the 2 offset experiments. The 2 data sets are denoted with red and blue colors, respectively.

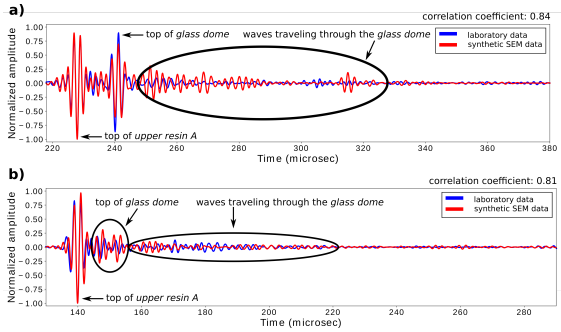


**Figure 11**. Comparison of offset lab traces with the corresponding synthetic SEM results: a) trace D, b) trace E.

ties and their own impacts on the misfits. Three kind of factors which possibly contribute to the observed misfits can be distinguished: those related exclusively to the experiments, those related exclusively to the numerical simulations, and those concerned with both the experimental and the numerical sides.

The reduced-scale experiments are of physical nature. Hence, similar to field data, our lab data still contain noise, although each signal was stacked several hundreds of times before being recorded, in order to enhance the signal-to-noise ratio and to remove any spurious incoherent noise. The presence of noise may be problematic mainly in offset configurations where signals can have very low amplitudes, but it can be partially removed by applying appropriate denoising methods. Nevertheless, noise is far from being the main issue we have to face here in our experimental work. Indeed, although the precision of the lab measurements has been significantly improved compared to those reported in [6], there is still a too high uncertainty in the initial transducer positions before the data acquisition. This uncertainty (of about $0.5\,mm$) has to be definitely investigated in details and decreased in future works, probably with the help of metrology, in order to drastically decrease the observed misfits between numerical results and experimental data.

In the numerical simulations the highly complex model geometry has been implemented using an equidistant grid which cannot explicitly honor the model discontinuities, in particular the sides of the dome and the junctions of the different resin layer boundaries next to the flanks of the dome. Nevertheless, the good fit observed for the reflections from the curved top surface of the glass dome, in both zero-offset and offset configurations, provides a reassuring feedback on the current implementation of the model geometry. Therefore, we consider this effect to be minimal if any.

On the contrary, two factors have much greater impact on the quality of the fit between numerical simulations and lab data: the numerical implementation of the source characteristics and that of the material properties. As already pointed out in [6], the implementation of the source characteristics used here does not describe perfectly the real directivity of the transducer and its full waveform (since the later arrivals of the wavelet are poorly reconstructed). Indeed, although the strongly energetic main lobe of the source transducer is very well restored (as it can be seen from the good fit between numerical and experimental data in zero-offset configuration), the lower-energy secondary lobes are poorly recovered by the inversion strategy proposed in [6] which seems to be inadequate in case of low signal-to-noise ratios. Therefore, further work must be done both from a theoretical point of view in order to improve the strategy, and from the experimental side to maximize the signal-to-noise ratio in the directivity measurements.

Before simulating wave propagation in the complex WAVES model, we have performed a numerical calibration of the material properties, consisting of the adjustment of the velocity and attenuation values such that there is a perfect fit between the chosen lab traces and the corresponding numerical ones. This preliminary and quite common procedure is necessary as the uncertainties are quite high in the lab characterization of the material properties, especially for the attenuation. However, we could observe that the obtained material properties are significantly influenced by the model area which is illuminated by the transducer beam. In future works, it would be particularly worthwhile to better understand this attenuation issue, both from theoretical and experimental aspects.

At this point, one last question should be raised: has the reduced-scale model been perfectly manufactured according to the initial 3D plans? Indeed, it is highly challenging to find the optimal process for manufacturing such a complex model and to ensure a perfect contact between the different material layers. A good way to check the quality of both the model and our “imperfect” experimental framework is to apply the reverse-time migration (RTM) to the lab data. For the sake of brevity, we will not present here the results obtained by the successfull aplication of RTM to the lab datasets, but the quality of these results validates the whole framework and confirms the high potential of laboratory experiments for cutting-edge seismic imaging and acquisition issues in complex environments.

## 5. CONCLUSIONS

The goal of this work was to provide a global reflection on the framework to be implemented to obtain high-quality laboratory data in the context of offshore seismics, regard-

less of the geological environment studied. To illustrate it, we have relied on a reduced-scale model representing a 3D complex-shaped salt body buried in sedimentary layers with curved surfaces. This model is made of a specific crystal, different resins with aluminum and silicon powders, and aluminum. Zero-offset and offset reflection data have been collected for this model in a water tank, using a conventional pulse-echo technique. Following our previous works, the framework has been defined using a cross-validation approach which allows, through the comparison between the experimental data and the numerical simulation of wave propagation, to point out both the improvements of the experimental setup which must still be made to increase the accuracy (and decrease the uncertainties) of the experiments, and the limitations of the numerical tool used (here, a spectral-element method) which must be tackled. For instance, inaccuracies in the initial position of sources and receivers before acquisition, the numerical implementation of the source directivity pattern, and high uncertainties in the estimation of the media properties (in particular, attenuations) may have a major impact on the quality of the proper use of laboratory data for imaging purposes. These issues can be solved with the help of metrology insights. On the contrary, the quality of the meshing of the complex model and the presence of noise, which can be removed by using proper signal processing techniques, have a low impact. The quality of both the complex reduced-scale model and the global framework proposed here has been successfully validated. Benefiting from recent (and future) technological advances, we believe that in the coming years, laboratory experiments can play a major role, in support of field experiments and numerical modeling, to explore some of the current challenges of seismic imaging in terms of, for instance, acquisition design or benchmarking of new imaging techniques at a low cost and in an "agile" way.

## 6. ACKNOWLEDGMENT

The WAVES model could be manufactured thanks to the enthusiasm, the involvement and the expertise of several persons and companies. The authors are very grateful to V. Long (LMA Marseille), La Fonderie du Verre (O. Fonderflick) and VN Composites (N. and J.-P. Tronquoy) who all have done a great job. The authors also thank V. Long, G. Machado, H. Abbadi, R. Guillermin, E. Debieu, G. Rabau and Ph. Lasaygues (LMA Marseille) for their valuable assistance in lab experiments and meshing. This work received funding from the European Union Horizon 2020 research and innovation program under the Marie Sklodowska-Curie grant, agreement no. 641943. B. Ursin thanks the Norwegian Research Council and the industry partners of the GAMES consortium for financial support (grant no. 294404). N. Favretto-Cristini thanks CNRS for financial support through the PICS BENCHIE project. This work was granted access to the French HPC resources of TGCC under allocation no. 2017-gen7165 made by GENCI.

## 7. REFERENCES

[1] T. Becker, D.-J. van Manen, C. Donahue, C. Baerlocher, N. Boersing, F. Broggini, T. Haag, J. A. Robertsson, D. Schmidt, S. Greenhalgh, and T. Blum, "Immersive wave propagation experimentation: physical implementation and one-dimensional acoustic results," *Physical Review X*, vol. 8, p. 031011, 2018.

[2] C.-H. Chang, Y.-F. Chang, and P.-Y. Tseng, "Azimuthal variation of converted-wave amplitude in a reservoir with vertically aligned fractures - a physical model study," *Geophysical Prospecting*, vol. 65, no. 1, pp. 221–228, 2017.

[3] X. Chai, S. Wang, J. Wei, J. Li, and H. Yin, "Reflectivity inversion for attenuated seismic data: Physical modeling and field data experiments," *Geophysics*, vol. 81, no. 1, pp. T11–T24, 2015.

[4] F. Bretaudeau, D. Leparoux, O. Durand, and O. Abraham, "Small-scale modeling of onshore seismic experiment: A tool to validate numerical modeling and seismic imaging methods," *Geophysics*, vol. 76, no. 5, pp. T101–T112, 2011.

[5] A. Tantsereva, B. Ursin, N. Favretto-Cristini, P. Cristini, and A. Aizenberg, "Numerical modeling of 3d zero-offset laboratory data by a discretized kirchhoff integral method," *Geophysics*, vol. 79, no. 2, pp. T77–T90, 2014.

[6] B. Solymosi, N. Favretto-Cristini, V. Monteiller, D. Komatitsch, P. Cristini, B. Arntsen, and B. Ursin, "How to adapt numerical simulation of wave propagation and ultrasonic laboratory experiments to be comparable - a case study for a complex topographic model," *Geophysics*, vol. 83, no. 4, pp. T195–T207, 2018.

[7] N. Favretto-Cristini, A. Aizenberg, B. Ursin, P. Cristini, and A. Tantsereva, "Analysis of wave scattering from a viscoelastic layer with complex shape," *Journal of Computational Acoustics*, vol. 25, no. 3, pp. 1750023–1–1750023–12., 2017.

[8] D. Pageot, D. Leparoux, M. L. Feuvre, O. Durand, P. Côte, and Y. Capdeville, "Improving the seismic small-scale modelling by comparison with numerical methods," *Geophysical Journal International*, vol. 211, pp. 637–649, 2017.

[9] Y. Liu, H. Hu, X.-B. Xie, Y. Zheng, and P. Li, "Reverse-time migration of internal multiples for subsalt imaging," *Geophysics*, vol. 80, no. 5, pp. S175–S185, 2015.

[10] D. Komatitsch and J.-P. Vilotte, "The spectral element method: an efficient tool to simulate the seismic response of 2d and 3d geological structures," *Bulletin of the Seismological Society of America*, vol. 88, no. 2, pp. 368–392, 1998.